Biogeosciences Discuss., 5, 1933–1967, 2008
www.biogeosciences-discuss.net/5/1933/2008/

Biogeosciences Discussions

Biogeosciences Discussions is the access reviewed discussion forum of *Biogeosciences*

Constraints on mechanisms and rates of anaerobic oxidation of methane by microbial consortia: process-based modeling of ANME-2 archaea and sulfate reducing bacteria interactions

B. Orcutt[1,2] **and C. Meile**[1]

[1]Department of Marine Sciences, University of Georgia, 30602 Athens, GA, USA
[2]Marine Environmental Biology Section, University of Southern California, 90089 Los Angeles, CA, USA

Received: 7 April 2008 – Accepted: 7 April 2008 – Published: 9 May 2008

Correspondence to: C. Meile (cmeile@uga.edu)

Published by Copernicus Publications on behalf of the European Geosciences Union.

Abstract

Anaerobic oxidation of methane (AOM) is the main process responsible for the removal of methane generated in Earth's marine subsurface environments. However, the biochemical mechanism of AOM remains elusive. By explicitly resolving the observed spatial arrangement of methanotrophic archaea and sulfate reducing bacteria found in consortia mediating AOM, potential intermediates involved in the electron transfer between the methane oxidizing and sulfate reducing partners were investigated via a consortium-scale reaction transport model that integrates the effect of diffusional transport with thermodynamic and kinetic controls on microbial activity. Model simulations were used to assess the impact of poorly constrained microbial characteristics such as minimum energy requirements to sustain metabolism, substrate affinity and cell specific rates. The role of environmental conditions such as the influence of methane levels on the feasibility of H_2, formate and acetate as intermediate species, and the impact of the abundance of intermediate species on pathway reversal was examined. The results show that higher production rates of intermediates via AOM lead to increased diffusive fluxes from the methane oxidizing archaea to sulfate reducing bacteria, but the build-up of the exchangeable species causes the energy yield of AOM to drop below that required for ATP production. Comparison to data from laboratory experiments shows that under the experimental conditions of Nauhaus et al. (2007), neither hydrogen nor formate is exchanged fast enough between the consortia partners to achieve measured rates of metabolic activity, but that acetate exchange might support rates that approach those observed.

1 Introduction

Methane, a potent greenhouse gas, is produced in anoxic regions of the ocean's subsurface and is largely prevented from entering the overlying water column and reaching the atmosphere by the activity of microorganisms living in marine sediments. Geo-

chemical evidence indicates that the net consumption of methane (CH_4) in these anoxic environments is linked to the consumption of sulfate (SO_4^{2-}; Barnes and Goldberg, 1976; Devol et al., 1984; Hoehler et al., 1994; Iversen and Jørgensen, 1985; Reeburgh, 1976):

$$CH_4 + SO_4^{2-} \rightarrow HS^- + HCO_3^- + H_2O \quad (1)$$

Results from DNA- and lipid-based investigations indicate that the consumption of sulfate and methane is mediated via a syntrophic relationship between sulfate-reducing bacteria (SRB) and methanotrophic archaea (ANME, after ANaerobic MEthanotroph; Hinrichs et al., 1999). Three distinct phylogenetic clades of ANMEs (ANME-1, -2, and -3; Knittel et al., 2005) and multiple SRB groups (Knittel et al., 2003) have been identified which may be involved with this process.

To date, significant gaps remain in understanding the biochemical mechanism of anaerobic oxidation of methane (AOM), including how the processes of AOM and sulfate reduction (SR) are linked to one another (Hoehler et al., 1994; Nauhaus et al., 2002; Sørensen et al., 2001; Valentine and Reeburgh, 2000). The concentrations of potential intermediates (Table 1) involved in electron exchange, produced during methane oxidation and consumed during sulfate reduction, likely play a significant role in regulating consortium energetics, as high concentrations thermodynamically favor SR but lower the energy yield for the ANME. Thus, a consortium relying on these two processes for energy production can only function within a certain range of concentrations of the intermediate compound, unless production and consumption are spatially separated enough to allow for a sufficient concentration difference between regions of active AOM and SR. Based on free energy yields in a setting with diffusive exchange of intermediates between an ANME and a nearby SRB cell, Sørensen et al. (2001) suggested that hydrogen and acetate are not feasible intermediates at low methane concentrations (tens of μM, representative of shallow water sediment environments). Arguing for lower in situ maintenance energy requirements of the consortia than those considered by Sørensen et al. (2001), Strous and Jetten (2004) determined that acetate is a thermodynamically favorable intermediate in settings with abundant methane

(>10 mM, such as CH_4 seep environments), while exchange of formate is thermodynamically feasible at lower methane concentrations.

Knowledge of the biochemical mechanism of AOM is limited since attempts to isolate these microorganisms in culture have so far been unsuccessful (Nauhaus et al., 2002). Nonetheless, some clues about the kinetic properties of the process can be derived from studies with environmental samples enriched in AOM-mediating microbes. For instance, cell specific rates of AOM can be inferred by comparing measurements of AOM activity in bulk samples with the corresponding abundance of cells assumed to be responsible for the process. Cell specific rates of AOM on the order of 10^{-4} to 10 fmol methane oxidized cell^{-1} d^{-1} can be inferred from a variety of datasets (Girguis et al., 2003, 2005; Knittel et al., 2005; Nauhaus et al., 2002; Orcutt et al., 2005); similarly, cell specific rates of SR in the environment are estimated to range from 10^{-2} to 10 fmol sulfate reduced cell^{-1} d^{-1} (as reviewed in Neretin et al., 2007).

Here we re-evaluate thermodynamic and kinetic constraints on the functioning of an ANME-2/SRB consortium by modeling the distribution of the chemical species involved in AOM at the scale of the consortium (<25 µm), including a number of substances that have been hypothesized to be exchanged between the ANME and the SRB. Three factors potentially govern the sustained rate of methane oxidation in a consortium: (1) the availability of substrate, where high reactant concentrations favor the reaction kinetically; (2) the energy yield of the reaction, where low product concentrations favor the reaction; and (3) the efficiency of transport of the exchangeable species from the zone of AOM (where it is produced) to the SRB (where it is consumed). By resolving the spatial arrangement of the methane oxidizing archaea and the sulfate reducing bacteria in the microbial aggregate, and by explicitly taking into account transport, reaction kinetics and thermodynamic constraints, we expand on and refine a previous assessment of requirements associated with intercellular exchanges by Sørensen et al. (2001), and a recent bulk analysis by Dale et al. (2006). We systematically vary poorly constrained parameters and assess the resulting process rates per aggregate. Specifically, we (i) study the impact of diffusion on the overall process energetics for

aggregates of different sizes; (ii) assess the role of minimum energy requirements for the functioning of the consortia; (iii) investigate the thermodynamic feasibility of a number of proposed intermediates; and (iv) consider thermodynamic constraints and the potential for a pathway reversal of the archaea under a variety of environmental conditions. These intrinsic microbial factors are discussed in the context of different environmental settings, in particular methane concentrations. Finally, model results at the consortium scale are compared with available laboratory rate data measured in ANME-2/SRB consortia enriched from a Hydrate Ridge methane seep (Nauhaus et al., 2007). We estimate maximum process rates per aggregate, and assess the likelihood for the different intermediates to give rise to the observed rates.

2 Model implementation

2.1 Consortium arrangement

While a variety of spatial arrangements of the syntrophic partners have been described (Knittel et al., 2005; Orphan et al., 2001, 2002), one of the predominant AOM-mediating ANME/SRB consortia is found in a spherical arrangement in which SRB form a shell around an inner core of archaea belonging to the ANME-2 cluster, presumably spatially separating SR from AOM (Fig. 1). From a survey on "shell-type" consortia sizes, cell sizes, and ANME:SRB abundance ratios, which were determined via 16S rRNA-based fluorescence in situ hybridization methods (Boetius et al., 2000; Knittel et al., 2003, 2005; Nauhaus et al., 2007; Orphan et al., 2001), a few trends emerge (Table 2). First, ANME-2 and SRB cells identified in these consortia tend to be 0.5 and 0.4 µm in diameter, respectively. Second, the ratio of the radius of the zone of ANME to the entire aggregate remains close to 0.73. Dividing the shell volumes by the respective average cell volumes leads to 3 SRB cells for every 1 ANME cell.

The model represents an individual aggregate, placed into an environment of radius r_{env} set to at least twice the aggregate radius (Fig. 1). At the outer edge of the model do-

main consisting of the aggregate and its surroundings, the concentrations are imposed to reflect those measured in field samples (Table 3). Alternatively, if the activity of the consortia determines the concentration of a chemical in the surrounding environment, it is assumed that the concentration gradient approaches zero at the domain boundary, as may be the case for the exchangeable species. Making use of symmetries, the computational domain is defined as a quadrant of a circle, which when rotated about a vertical axis and mirrored horizontally approximates the spherical physical domain.

2.2 Governing equations

The concentrations of dissolved chemical species (C_i) are subject to diffusion within the free fluid fraction of the consortium, and production/consumption reactions:

$$\phi \frac{\partial C_i}{\partial t} = \nabla \cdot (\phi D \nabla C_i) + \phi R \quad (2)$$

where t is time, ϕ is porosity which is set to 0.3 within the consortium – a value slightly above that for densest packing of spherical cells (0.26; Martin et al., 1997) – and 1 in the surrounding pore water, D is the in situ diffusion coefficient, and R equals the net of production and consumption terms of species i. Equation (2) is implemented in the finite element simulation environment COMSOL® and solved for steady state using a direct solver (UMFPACK). The chemical species considered here include methane (CH_4), dissolved inorganic carbon, sulfide, sulfate (SO_4^{2-}) and the exchangeable species, (i.e. H_2, formate, acetate; Table 1).

In situ diffusion coefficients are based on measures of molecular diffusion in dilute solutions at 8°C (D_{aq}, Table 3). Aggregates are typically embedded in a thick organic matrix (Knittel et al., 2005; Orphan et al., 2001). Estimating its effect on diffusion from experiments with extracellular polymers, the diffusion coefficient is reduced by a factor f_{eps}, set to 0.25 for organic ions and to 0.6 for inorganic ions and gases (Stewart, 2003). The presence of cells is taken into account via a tortuosity correction, so that the in situ

diffusion coefficient is defined as:

$$D = f_{\text{eps}} \frac{D_{\text{aq}}}{\theta^2} \tag{3}$$

where the tortuosity factor θ^2 is set to 2.5. This is at the lower end of tortuosity values suggested from porosity-tortuosity datasets (Boudreau, 1997), but leads to values of effective diffusion coefficients at the lower end of the range determined experimentally in microbial mats (Wieland et al., 2001).

2.3 Reactions and rate laws

The reactions in AOM and SR zones can be generalized as follows:

$$CH_4 \rightarrow EX + HCO_3^- \tag{4}$$

$$SO_4^{2-} + EX \rightarrow HS^- \tag{5}$$

where EX represents the intermediate species which acts as the electron carrier between AOM and SR (Table 1). AOM occurs exclusively within the inner sphere of ANME in the aggregate while SR is restricted to the outer shell of the aggregate. The rate laws contain a Monod-type dependence on the substrates of each reaction and account for environmental conditions via a factor (F_T) that depends on the cell's energy yield:

$$R_{\text{AOM}} = k_{\text{AOM}} B_{\text{ANME}} \frac{[CH_4]}{Km CH_4 + [CH_4]} F_{T-\text{AOM}} \tag{6}$$

$$R_{\text{SR}} = k_{\text{SR}} B_{\text{SRB}} \frac{[EX]}{Km EX + [EX]} \frac{[SO_4^{2-}]}{Km SO_4 + [SO_4^{2-}]} F_{T-\text{SR}} \tag{7}$$

where R_{AOM} and R_{SR} are the AOM and SR rates (in units of nmol $cm^{-3}\,d^{-1}$), respectively; k_{AOM} and k_{SR} are the corresponding maximum cell specific rate constants (nmol

cell^{-1} d^{-1}); B_{ANME} and B_{SRB} are the cell densities of ANME in the inner core and SRB within the outer shell of the consortium (cells cm^{-3}), respectively; [C_i] represents the concentration of species i; $Km CH_4$, $Km EX$ and $Km SO_4$ are the half-saturation constants for methane, the exchangeable species and sulfate, respectively; and F_{T-AOM} and F_{T-SR} are the "thermodynamic potential" factors (Jin and Bethke, 2003, 2007) for AOM and SR, respectively.

Baseline values of various parameters are presented in Table 4. All cells are assumed to have the same maximum turnover potential such that k_{AOM} and k_{SR} are population specific constants. Half saturation constants for the exchangeable species are assumed to be on the order of typical concentration ranges measured in the environment, as may be the case for SRB adapted to in situ conditions and able to respond to perturbations in substrate availability. For example, $Km H_2$ is varied in the nanomolar range (Table 4), reflecting measured hydrogen concentrations in or around the zone of AOM typically range from 0.1–1 nM (Finke, 2003; Hoehler et al., 1994, 1998) and previous estimates of half saturation constants in coastal marine sediments of 10 nM H_2 (Dale et al., 2006). Km values for sulfate and methane were chosen to be similar to previous investigations (Dale et al., 2006) and are comparable to values calculated from experimental data (T. Treude, A. Boetius, personal communication).

The thermodynamic potential factors (F_{T-X}, where X represents either AOM or SR) reflect that there must be sufficient free energy available from the reactions to fuel ATP synthesis and cell maintenance. For instance, if the concentration of the intermediate species made AOM energetically unfavorable, regardless of the availability of methane for consumption, methane oxidation is assumed not to take place. F_{T-X} is defined as:

$$F_{T-X} = \max\left(0, 1 - \exp\left(\frac{f_X}{\chi R_g T}\right)\right) \quad (8)$$

where χ, the number of ATP synthesized per reaction, equals 1, R_g is the universal gas constant (8.314 J K^{-1} mol^{-1}) and T is the absolute temperature (281.15 K). f_X represents the thermodynamic driving force for reaction X, relating the free energy yield

of that reaction to the energy required to synthesize ATP (Jin and Bethke, 2003, 2007) and is determined as:

$$f_X = -\Delta G_X - m\Delta G_{\mathrm{ATP}} \quad (9)$$

Here, ΔG_X is the free energy yield of reaction X under in situ conditions, i.e.

$$\Delta G_X = \Delta G_X^0 + RT \ln\left(\prod a_i^{v_i}\right) \quad (10)$$

ΔG_X^0 is the standard free energy of reaction, determined from the free energy of formation of the species involved in the reactions (Table 3), a_i represents the activity of species i, computed based on the modeled concentrations and the activity coefficients given in Table 3, and v_i are the stoichiometric coefficients. m in Eq. (9) is the number of ATP synthesized per electron transferred. Direct measurements of m for AOM do not exist, as no pure cultures of AOM-mediating microorganisms can be manipulated for such a study. Available genomic data indicate that AOM may occur via a reversal of the enzymatic process of methanogenesis (Hallam et al., 2003, 2004; Krüger et al., 2003), thus we estimate m based on available data from methanogenic archaea, presented by Duppenmeier (2002). In methanogenesis, the final enzymatic step catalyzed by methyl coenzyme A reductase creates a heterodisulfide of coenzymes B and S. The cleavage of this heterodisulfide by oxidoreductases fuels electron transport in the cell, which is accompanied by proton translocation (4 H^+/2 e^-) and drives ATP synthesis. Thus, there is 1 ATP synthesized per 2 electrons transported, and $m{=}\frac{1}{2}$. ΔG_{ATP} in Eq. (9) represents the threshold energy limit for growth, which is often assumed to be the energy required to synthesize ATP. Assuming ~60 kJ/mol ATP to form ATP from ADP and phosphate and that three protons are translocated per ATP produced (Schink, 1997; Thauer, 1977), this energetic limit is on the order of 20 kJ/mol H^+, though it has been shown experimentally that some methanogens can survive with a free energy yield of 12–16 kJ/mol H^+ (Jackson and McInerney, 2002), and even lower threshold energy limits of 4 kJ/mol H^+ have been proposed (as reviewed in Dale et al., 2006). In our model,

a range of $m\Delta G_{ATP}$ values from 1–10 kJ/mol H^+ is considered. Note that Eq. (8) restricts the value of F_{T-X} to the range between 0 and 1 and does not allow for a net back reaction.

In situ energy yield (Eq. 10) depends on the activities of individual compounds and hence chemical speciation. For a solution containing Ca^{2+}, K^+, Mg^{2+}, Na^+, Cl^-, SO_4^{2-} at concentrations of seawater, 1 mM sulfide and 2 mM dissolved inorganic carbon, and the potential intermediates acetate and formate present at micromolar levels, the CH_3COO^- and $HCOO^-$ species constitute more than half the total concentrations over a range of pH 5 to 9. Though the impact of organics in the intercellular space is not known, simulations in which only a 10% fraction of the total intermediate concentrations is considered in free form when calculating F_T suggest that speciation of the exchangeable species may not be the dominant control on the process energetics (not shown). Variations relevant to the calculation of the in situ ΔG_{rxn} result from the relative distribution of the acid-base species H_2CO_3–HCO_3^-–CO_3^{2-} and H_2S–HS^-–S^{2-}, respectively. Below, we assume a spatially uniform pH of 8, so that bicarbonate and hydrogen sulfide are the dominant forms of dissolved inorganic carbon and sulfide.

3 Results and discussion

To quantify thermodynamic and kinetic influences on the rates of AOM performed by the ANME/SRB shell-type consortia, model simulations were conducted in which poorly constrained parameter values were varied systematically. To facilitate comparison of model results, volume averages of the parameters for the inner ANME core or the outer SRB shell are presented. Simulations that result in conditions with drastic changes at or below the scale of individual cells, e.g. complete thermodynamic inhibition of AOM within one cell diameter distance from the zone of SR, are not included in the analysis. As our simulations consistently indicated much stronger thermodynamic challenges for the ANME compared to the SRB, the presentation of the results highlights the sensitivity of F_{T-AOM} and the rate of AOM towards poorly constrained process parameters.

The AOM results presented focus on the maximum allowable cell specific rates of AOM, which corresponds to the highest rates of AOM that can be achieved for a given set of reaction conditions before the reaction zone collapses to the thickness of a cell due to thermodynamic limitation.

3.1 Impact of transport intensity and aggregate size

Diffusive transport counteracts the build up of the exchangeable species within the inner core of the consortia and provides the SRB with substrate. Given the critical role of transport of the exchangeable species from the location of production to the zone of sulfate reduction, the poorly constrained influence of the organic matrix on diffusive transport was investigated. Removing the impact of EPS on diffusion lessened thermodynamic limitation (i.e. higher $F_{T-\mathrm{AOM}}$ without EPS). However, even for organic ions with a low value of f_{eps}, the magnitude of the change was not large enough to significantly modify the consortia's methane consumption rate.

Aggregates vary in size from a few to tens of micrometers (Table 2), and such a difference in spatial dimension may impact the distribution of chemicals and turnover rates in the consortium. Model simulations show that for a given set of kinetic parameters, aggregate size can significantly affect the magnitude of rates of AOM, with higher rates and lower thermodynamic limitation occurring in the smaller aggregates. For example, Fig. 2 displays the differences in maximum AOM rates for variously sized aggregates (3, 12 and 25 µm consortium diameters) assuming acetate, formate or hydrogen as the exchangeable species. In all cases, the half saturation constant for the exchangeable species was assumed to be 100 nM, which corresponds to a value that is 1–100 times the average concentration at steady state in the inner core of the aggregate. For any given aggregate size and assumed cell specific rate of AOM, the thermodynamic limitation of AOM decreases with increasing cell specific rate of SR, which is reflected in the increasing rate of AOM. For each exchangeable species considered, the maximum cell specific rate of AOM decreases with increasing size of the aggregate, indicating that AOM becomes less favorable as the consortia grow in size. Additionally, at these

cell specific turnover rates, $F_{T-\mathrm{AOM}}$ is homogenous in the smaller consortia, while in the larger ones $F_{T-\mathrm{AOM}}$ shows a pronounced gradient with higher values next to the contact with the SRB shell (not shown). For consortia larger in size (25 vs. 12 and 3 µm, Fig. 2), some of the areas of production of the exchangeable species are too far away from the SRB; thus, the exchangeable species cannot diffuse out of the inner core fast enough to prevent its build up to a level that lowers the available free energy yield below what is necessary for maintaining cell activity. As the smaller sized consortia are numerically more abundant in experimental observations (Table 5), the remainder of the simulations focused on the smallest size class (i.e. 3 µm diameter aggregates).

In addition to their size, the (possibly patchy) spatial distribution of the aggregates within the sediment matrix may also affect bulk AOM rates. For a typical aggregate density of 10^7 per cm^3, aggregates are typically 10–100 µm apart. However, F_T was found to vary little with the size of r_{env}. Even when imposing aggregate distances on the order of 1 µm, implying a clustered and uneven distribution, and when imposing high exchangeable species concentrations – assumed to be maintained by processes external to the aggregates – at the outer domain boundary, $F_{T-\mathrm{AOM}}$ is only slightly diminished (not shown). This indicates that the distribution of aggregates in otherwise homogeneous sediments does not influence the energetics of AOM significantly.

3.2 Kinetic and thermodynamic controls on reaction rates

In the absence of experimental data on the nature of the intermediate species of coupled AOM/SR and the associated kinetic parameters, the impact of rate and half saturation constants on AOM activity and thermodynamic limitations was investigated. For each of the three potential intermediates considered, model simulations were run in which the maximum cell specific rates of AOM and SR, k_{AOM} and k_{SR}, were varied. In addition, the values for the half saturation constants of sulfate reducers for the intermediate compounds (i.e. K_mEX) were also systematically varied. Rates increase with increasing k_{AOM}, until at high k_{AOM} values diffusion is too slow to prevent build up of products in the zone of AOM, leading to thermodynamic shutdown of the reac-

tion in the center of the aggregate. The value of this maximum cell specific rate of AOM differs between the potential intermediates and depends on the environmental conditions and aggregate size (Figs. 2, 3 and 4). For example, under high (100 mM) methane conditions, k_{AOM} can reach as high as 1 fmol cell^{-1}d^{-1} when acetate is the exchangeable species (Fig. 3a), while with formate and hydrogen, k_{AOM} is limited to 10^{-2} fmol cell^{-1} d^{-1} (Fig. 3d and g).

The point at which the sulfate reduction rate exceeds the delivery of the exchangeable species (i.e. SR uses up all substrates within a zone smaller than a cell diameter, Fig. 3k) varies between the considered compounds. This can be explained by the stoichiometry of the AOM/SR reactions and by differences in diffusion coefficients of the intermediate compounds. For example, with a cell specific AOM rate of 0.01 fmol cell^{-1} d^{-1}, a ΔG_{ATP} of 1 kJ mol^{-1} and a $K m$EX of 10 µM, the maximum cell specific rate of SR for acetate is approximately 200 fmol cell^{-1} d^{-1}, whereas for formate the maximum cell specific rate of SR is around 30 fmol cell^{-1} d^{-1}. The diffusion and activity coefficients of formate and acetate are similar (Table 3), yet for every methane molecule consumed, there are 4 formate molecules produced as opposed to 1 acetate molecule. The higher production of formate per methane can lead to a higher availability of substrate for the SRB, and the reduced substrate limitation increases SR rates at the ANME-SRB interface, causing a narrowing of the SR zone at lower cell specific rates. Hydrogen and formate exhibit the same substrate-to-intermediate stoichiometry (four molecules of intermediate per methane molecule), yet the maximum cell specific rate of SR for hydrogen is higher than for formate at 300 fmol cell^{-1} d^{-1}, which can be explained by the higher diffusion coefficient of hydrogen than of formate (Table 3).

AOM activity is highest at a balance between k_{SR} and the relative abundance of exchangeable species, here expressed as the ratio of the half saturation constant and the average concentration of the exchangeable species in the aggregate core at steady state (denoted as $K m$EX/[EX]; Fig. 3). The roughly linear log-log relationship between the cell specific rate of SR (i.e. k_{SR}) and the ratio of the half saturation constant to the steady state concentration of the intermediate species holds whenever the half

saturation constant is greater than or equal to the calculated steady state concentration of the intermediate compound, so that $R_{SR} \approx k^*_{SR} B_{SRB} F_{T-SR}$, where the effective rate constant $k^*_{SR} \approx k_{SR}/(K_m EX/EX)$ is on the order of $k_{AOM}/10$. Notably, the linear log-log relationship between these two parameters that give rise to maximum AOM rates passes through the range of values expected from observations (i.e. shaded regions in Figs. 3 and 4).

The highest rates per aggregate are typically achieved when part of the ANME are inactive due to thermodynamic constraints (not shown). For a fixed value of k_{AOM} and a given ratio of the half saturation constant to the steady state concentration of the exchangeable species in the aggregate core, the rate of AOM increases with increasing cell specific rates of SR (Fig. 3). This is not because of a change in the availability of AOM substrates, but because increasing k_{SR} promotes depletion of EX near the zone of AOM, which leads to a more efficient removal and lower levels of EX in the aggregate core. Hence, the increase in k_{SR} improves thermodynamic favorability of the AOM reaction. Similarly, an increased $K_m EX/[EX]$ ratio reflects a relative decrease of EX in the inner core, alleviating thermodynamic constraints active at high rates. This pattern holds until a point is reached in which the rate of SR is too high to be sustained by the delivery via diffusion of the exchangeable species from AOM (Fig. 3k). Thus, although AOM is energetically still favorable, the zone where substrate for SR is available becomes smaller than a cell diameter, which is considered a lower limit.

Previous examinations of the syntrophic AOM/SR consortia indicate that due to the impact of methane concentration of the free energy yield of AOM, methane availability may determine which compounds can be feasible electron shuttles (Sørensen et al., 2001; Strous and Jetten, 2004; Valentine, 2002). Acetate, and to some degree hydrogen, have been considered feasible intermediates in the AOM/SR syntrophy at elevated methane concentrations (high mM range), whereas formate might lead to favorable AOM at lower methane concentrations. As shown in Fig. 3 and Table 6, our simulations indicate that AOM is thermodynamically favorable for all three potential intermediate compounds when the combination of kinetic parameters allows for efficient

removal of the exchangeable species from the zone of AOM, and when the assumed energy threshold is relatively low (i.e. ΔG_{ATP} is 1 kJ/mol; see below for further discussion about the impact of varying the energy threshold). Under the range of parameters tested here, the calculated rates of AOM per aggregate are highest when acetate is the intermediate species.

AOM dynamics with acetate as the exchangeable species vary more in relation to changes in methane concentration (Fig. 3a–c) than is observed for either formate (Fig. 3d–f) or hydrogen (Fig. 3g–i). For example, with acetate as intermediate, maximum rates drop by approximately an order of magnitude and the k_{AOM} corresponding to the maximum rates decreases pronouncedly with decreasing methane concentration from 1 fmol cell^{-1} d^{-1} at 100 mM CH_4 to 0.01 fmol cell^{-1} d^{-1} at 1 mM CH_4. By comparison, the change in the highest cell specific rates of AOM in relation to decreasing methane concentrations is from 0.01 to 0.001 fmol cell^{-1} d^{-1} for formate or not at all in the case of hydrogen.

An additional parameter influencing the thermodynamic limitation of AOM is the minimum free energy required to maintain life – the ΔG_{ATP}. The prior examples were calculated with an assumed ΔG_{ATP} of 1 kJ/mol electron, an exceptionally low value in comparison to typical assumed values that are closer to 20 kJ/mol. Figure 4 and Table 6 illustrate the impact of ΔG_{ATP} on the dynamics of AOM for the various intermediate species exchanged by a small consortium under a methane concentration of 19 mM. As observed above, the consortia modeled with acetate shows the most pronounced variance with changes in assumed energy requirements – as the energy threshold raises, the thermodynamic favorability and subsequent rate of AOM with acetate decreases significantly (Fig. 4a–c). The decrease in AOM rates with increasing energy threshold is less pronounced when formate (Fig. 4d–f) or hydrogen (Fig. 4g–i) are the modeled intermediate species.

3.3 What is the exchangeable species?

To determine which compound(s) can feasibly serve as the exchangeable species in AOM/SR syntrophy, modeled rates of AOM are compared to laboratory results gathered from a growth experiment with ANME-2 – Desulfosarcina/Desulfococcus shell-type consortia, enriched from a Hydrate Ridge methane seep and incubated with abundant (19 mM) methane (Nauhaus et al., 2007). In that experiment, a near ten-fold increase in AOM-mediating community abundance corresponded to an ~ten-fold increase in the rate of metabolic activity. At the end of the experiment the rate of activity in the enrichment was approximately 250 µmol (gram wet sediment, gws)$^{-1}$ d^{-1}, and the size distribution of the aggregates was recorded (Table 5). To compare model simulations with experimental values, the methane consumption for an aggregate of a given size is computed and then multiplied by the number of aggregates in that size class in 1 gram of sediment at the end of the Nauhaus experiment (Table 5). This approach takes into account the potential for reduced AOM rates in the center of larger aggregate and considers the relative contribution of that size aggregate to the total rate.

The above simulations evaluating the effect of the variation of intermediate species, maximum cell specific rates, substrate limitations and minimum energy requirements (Figs. 3 and 4) allows one to constrain the parameter space consistent with the observation. The highest rates of AOM per aggregate, approximately 650 µmol gws^{-1} d^{-1}, occur with acetate as intermediate, at a cell specific AOM rate of 1 fmol cell^{-1} d^{-1}, 100 mM methane and an energy threshold of 1 kJ/mol (Fig. 3a). The highest possible rates of AOM with hydrogen and formate under these same conditions are ~13 µmol gws^{-1} d^{-1}, and they occur at a lower cell specific AOM rate of 0.01 fmol cell^{-1} d^{-1}. For the simulations conducted with 19 mM CH_4, which corresponds to the methane concentration used in the Nauhaus experiments, but otherwise identical parameterization, the optimal cell specific rate of AOM is 0.1 fmol cell^{-1} d^{-1} when acetate is the intermediate species and 0.01 fmol cell^{-1} d^{-1} for formate and

hydrogen (Fig. 3b, e, and h). The corresponding AOM rates at this methane concentration are 85, 12 and 13 $\mu mol\,gws^{-1}\,d^{-1}$, for acetate, formate, and hydrogen, respectively, which is lower than the rate of activity measured in the experiment ($\sim$250 $\mu mol\,gws^{-1}\,d^{-1}$). These results indicate that, at high methane concentration, acetate yields the highest possible rates of AOM, which exceeds the measured ones, but under the experimental conditions the modeled rates are slightly lower than those observed.

3.4 Can ANME "switch" metabolic modes to produce methane for energy generation?

Experimental data allows for the possibility that some ANME perform methanogenesis under in situ conditions, although at a lower relative rate than that of AOM (Orcutt et al., 2005, 2008; Treude et al., 2007). Additional DNA and protein-based analyses indicate that ANME possess enzymatic machinery to allow methane oxidation via a reverse methanogenesis pathway (Chistoserdova et al., 2005; Hallam et al., 2004; Krüger et al., 2003). To test whether environmental conditions and/or consortia dynamics may influence whether ANME perform methane oxidation and/or methanogenesis under in situ conditions, the model was modified to allow the ANME to "switch" metabolic modes from methanotrophy to methanogenesis based on their local environment. For instance, under conditions of concurrent low methane and high hydrogen concentration, methanogenesis may become energetically favorable, and perhaps the ANME can take advantage of this and operate in reverse. In the absence of experimental data it is assumed that the rate of methanogenesis – Eq. (4) in reverse – proceeds at an intrinsic rate comparable to the one of methanotrophy and is also subject to thermodynamic constraints:

$$R_{MG} = k_{AOM} B_{ANME} F_{T-MG} \tag{11}$$

where F_{T-MG} is defined by Eq. (8) with $f_X = -f_{AOM}$.

Regardless of the exchangeable species considered, under no gradient conditions at the domain boundary (i.e. when the consortia controls the concentration of the

exchangeable species in the environment), the exchangeable species concentration within the consortia never reaches a high enough steady state value to make methanogenesis energetically favorable, regardless of aggregate size in the entire range considered (3 µm $< r_{agg} <$25 µm; data not shown). At high cell specific AOM values, AOM is basically shut down because of exchangeable species production, but concentrations never build up enough to cause a switch to methanogenesis.

In contrast, when the exchangeable species are forced to be at a certain concentration at the domain boundary, reflecting outside sources of the exchangeable species that are not modeled explicitly, the exchangeable species concentration in the AOM zone can reach values sufficiently high for reverse methanotrophy to become energetically feasible (Fig. 5). For example, at environmental hydrogen concentrations typical of AOM zones (<5 nM), methanogenesis is not favorable regardless of the corresponding rate of SR; conditions are favorable for AOM, as long as k_{AOM}<0.1 fmol cell^{-1} d^{-1}, above which the zone of activity (F_{T-AOM}>0) is smaller than the diameter of an ANME cell and therefore considered unrealistic (not shown). When the outside hydrogen concentration is 10–50 nM, a level more typical for deeper methanogenic sedimentary zones or possible in highly reduced fluids, the steady state hydrogen concentration within the consortia is high enough to permit methanogenesis when the corresponding rate of SR is low, though rapid H_2 consumption (high k_{SR}) can still favor AOM. At even higher environmental hydrogen concentrations (greater than 100 nM), conditions are never favorable for AOM regardless of the speed of SR.

These trends are similar when acetate and formate are considered as the exchangeable species, although the specific concentrations leading to the trends vary slightly. For example, with acetate, AOM is always favorable until the concentration of the exchangeable species in the environment exceeds 25 nM; at concentrations greater than 100 nM, AOM never becomes favorable. AOM from formate starts to become limited when the formate concentration in the environment is forced to be 25 nM, and formate levels of 300 nM or higher are required to make AOM never favorable. Notably, at no instance are methanogenesis and methanotrophy observed simultaneously

within the ANME core. However, if EX concentrations in the environment flucuate temporally and vary by about an order of magnitude, a change from methane oxidation to methanogenesis cannot be ruled out based on the model results (transition from 25 to 150 nM acetate, 10 to 50 nM formate and 1 to 10 nM H_2, respectively, at k_{SR}=0.05 fmol cell^{-1} d^{-1}; Fig. 5).

4 Conclusions

Model simulations indicate that all investigated compounds – acetate, formate, and hydrogen – have the potential to sustain a syntrophic AOM/SR relationship under a range of methane concentrations and with various assumed thresholds for free energy. Examining the impact of poorly constrained parameters, including transport coefficients and the effect of chemical speciation revealed that these factors are unlikely to sufficiently alter the rate of AOM to a large enough degree to substantially change this finding. Of the three potential intermediate compounds, acetate was the only one that could generate modeled AOM rates that are comparable to observed values, albeit only if operating at a very low energetic threshold. In the absence of pure cultures, the metabolic capabilities of the syntrophic partners are insufficiently known to exclude the possibility for acetate to serve as the intermediate at millimolar methane concentrations. A number of factors could be invoked that facilitate higher in situ AOM rates, including intrinsic variations in cell specific rates across consortia sizes or substantial modification of the local chemical environment through active cross-membrane transport (e.g. proton pumps; spatial pH variations impact both formate and hydrogen, but less so acetate; Table 1). Alternatively, a more complex geometry than the one considered may facilitate contact between the syntrophic partners, or other physiological adaptations, including a network of nanowire-like structures (Reguera et al., 2006), that allows for a more efficient exchange between ANME and SRBs may alleviate the identified thermodynamic constraints. Our mechanistic, process-based model analysis and comparison to rates measured in laboratory incubation shows that all three factors –

reaction kinetics, transport intensities and energetic considerations – decisively impact the overall rate of methane consumption. The potential for significant spatial variability in substrate availability is predicted even over distances <10 µm, a finding to be corroborated e.g. by mapping regions of active growth and uptake of compounds with coupled FISH-SIMS. Balancing of transport and different reaction processes leaves room for a variety of mechanisms for the interaction between the consortium partners – including pathway reversal under fluctuating environmental concentrations of the exchangeable species, and alternatives to the three intermediates investigated here – and metabolic plasticity may prevail even in methane oxidizing consortia that live in environments with little excess energy.

Acknowledgements. We would like to thank Antje Boetius and Katja Nauhaus for sharing raw experiment data on consortia dynamics, and Samantha Joye for helpful discussion. This work was supported by a National Science Foundation Graduate Research Fellowship to B. Orcutt while at UGA and a fellowship from the Hanse Institute for Advanced Studies to C. Meile that provided hospitality and financial support in Delmenhorst, Germany. C. Meile also acknowledges support by the Office of Science of the United States Department of Energy (DE-FG02-05ER25676).

References

Barnes, R. O. and Goldberg, E. D.: Methane production and consumption in anaerobic marine sediments, Geology, 4, 297–300, 1976.

Boetius, A., Ravenschlag, K., Schubert, C. J., Rickert, D., Widdel, F., Gieseke, A., Amann, R., Jørgensen, B. B., Witte, U., and Pfannkuche, O.: A marine microbial consortium apparently mediating anaerobic oxidation of methane, Nature, 407, 623–626, 2000.

Boudreau, B. P.: Diagenetic models and their implementation, Springer-Verlag, 1997.

Chistoserdova, L., Vorholt, J. A., and Lidstrom, M. E.: A genomic view of methane oxidation by aerobic bacteria and anaerobic archaea, Genome Biology, 6(208), doi:10.1186/gb-2005-6-2-208, 2005.

Dale, A. W., Regnier, P., and van Cappellen, P.: Bioenergetic controls on anaerobic oxidation of methane (AOM) in coastal sediments: A theoretical analysis, Am. J. Sci., 306, 246–294, 2006.

Devol, A. H., Anderson, J. J., Kuivila, K., and Murrary, J. W.: A model for coupled sulfate reduction and methane oxidation in the sediments of Saanich Inlet, Geochim. Cosmochim. Ac., 48, 993–1004, 1984.
Duppenmeier, U.: Redox-driven proton translocation in methanogenic Archaea, Cell. Mol. Life Sci., 59, 1513–1533, 2002.
Finke, N.: The role of volatile fatty acids and hydrogen in the degradation of organic matter in marine sediments, Doctoral, University of Bremen, 2003.
Girguis, P. R., Cozen, A. E., and DeLong, E. F.: Growth and population dynamics of anaerobic methane-oxidizing archaea and sulfate-reducing bacteria in a continuous-flow bioreactor, Appl. Environ. Microb., 71(7), 3725–3733, 2005.
Girguis, P. R., Orphan, V. J., Hallam, S. J., and DeLong, E. F.: Growth and methane oxidation rates of anaerobic methanotrophic archaea in a continuous-flow bioreactor, Appl. Environ. Microb., 69(9), 5472–5482, 2003.
Hallam, S. J., Girguis, P. R., Preston, C. M., Richardson, P. M., and DeLong, E. F.: Identification of methyl coenzyme M reductase A (mcrA) genes associated with methane-oxidizing archaea, Appl. Environ. Microb., 69(9), 5483–5491, 2003.
Hallam, S. J., Putnam, N., Preston, C. M., Detter, J. C., Rokhsar, D., Richardson, P. M., and DeLong, E. F.: Reverse methanogenesis: Testing the hypothesis with environmental genomics, Science, 305, 1457–1462, 2004.
Hinrichs, K.-U., Hayes, J. M., Sylva, S. P., Brewer, P. G., and DeLong, E. F.: Methane-consuming archaebacteria in marine sediments, Nature, 398, 802–805, 1999.
Hoehler, T. M., Alperin, M. J., Albert, D. B., and Martens, C. S.: Field and laboratory studies of methane oxidation in an anoxic marine sediment – evidence for a methanogen-sulfate reducer consortium, Global Biogeochem. Cy., 8, 451–463, 1994.
Hoehler, T. M., Alperin, M. J., Albert, D. B., and Martens, C. S.: Thermodynamic control on hydrogen concentrations in anoxic sediments, Geochim. Cosmochim. Ac., 62, 1745–1756, 1998.
Iversen, N. and Jørgensen, B. B.: Anaerobic methane oxidation rates at the sulfate-methane transition in marine sediments from Kattegat and Skagerrak (Denmark), Limnol. Oceanogr., 30, 944–955, 1985.
Jackson, B. E. and McInerney, M. J.: Anaerobic microbial metabolism can proceed close to thermodynamic limits, Nature, 415, 454–456, 2002.
Jin, Q. and Bethke, C. M.: A new rate law describing microbial respiration, Appl. Environ.

Microb., 69(4), 2340–2348, 2003.
Jin, Q. and Bethke, C. M.: The thermodynamics and kinetics of microbial metabolism, Am. J. Sci., 307, 643–677, 2007.
Knittel, K., Boetius, A., Lemke, A., Eilers, H., Lochte, K., Pfannkuche, O., and Linke, P.: Activity, distribution, and diversity of sulfate reducers and other bacteria in sediments above gas hydrate (Cascadia Margin, Oregon), Geomicrobiol. J., 20, 269–294, 2003.
Knittel, K., Lösekann, T., Boetius, A., Kort, R., and Amann, R.: Diversity and Distribution of Methanotrophic Archaea at Cold Seeps, Appl. Environ. Microb., 71(1), 467–479, 2005.
Krüger, M., Meyerdiecks, A., Glockner, F. O., Amann, R., Widdel, F., Kube, M., Reinhardt, R., Kahnt, R., Bocher, R., Thauer, R. K., and Shima, S.: A conspicuous nickel protein in microbial mats that oxidize methane anaerobically, Nature, 426, 878–881, 2003.
Martin, I., Dozin, B., Quarto, R., Cancedda, R., and Beltrame, F.: Computer-based technique for cell aggregation analysis and cell aggregation in in vitro chondrogenesis, Cytometry, 28, 141–146, 1997.
Nauhaus, K., Albrecht, M., Elvert, M., Boetius, A., and Widdel, F.: In vitro cell growth of marine archaeal-bacterial consortia during anaerobic oxidation of methane, Environ. Microbiol., 9(1), 187–196, 2007.
Nauhaus, K., Boetius, A., Krueger, M., and Widdel, F.: In vitro demonstration of anaerobic oxidation of methane coupled to sulfate reduction from a marine gas hydrate area, Environ. Microbiol., 4, 296–305, 2002.
Neretin, L., Abed, R. M. M., Schippers, A., Schubert, C., Kohls, K., and Kuypers, M. M. M.: Inorganic carbon fixation by sulfate-reducing bacteria in the Black Sea water column, Environ. Microbiol., 9, 3019–3024, 2007.
Orcutt, B. N., Joye, S. B., Boetius, A., Elvert, M., and Samarkin, V. A.: Molecular biogeochemistry of sulfate reduction, methanogenesis and the anaerobic oxidation of methane at Gulf of Mexico cold seeps, Geochim. Cosmochim. Ac., 69(17), 4267–4281, 2005.
Orcutt, B. N., Samarkin, V., Boetius, A., and Joye, S. B.: On the relationship between methane production and oxidation by anaerobic methanotrophic communities from cold seeps of the Gulf of Mexico, Environ. Microbiol., 10(5), 1108–1117, doi:10.1111/j.1462-2920.2007.01526.x, 2008.
Orphan, V. J., Hinrichs, K.-U., Ussler III, W., Paull, C. K., Taylor, L. T., Sylva, S. P., Hayes, J. M., and DeLong, E. F.: Comparative analysis of methane-oxidizing archaea and sulfate-reducing bacteria in anoxic marine sediments, Appl. Environ. Microb., 67(4), 1922–1934, 2001.

Orphan, V. J., House, C. H., Hinrichs, K.-U., McKeegan, K. D., and DeLong, E. F.: Multiple archaeal groups mediate methane oxidation in anoxic cold seep sediments, P. Natl. Acad. Sci. USA, 99, 7663–7668, 2002.
Reeburgh, W. S.: Methane consumption in Cariaco Trench waters and sediments, Earth Planet. Sc. Lett., 28, 337–344, 1976.
Reguera, G., Nevin, K. P., Nicoll, J. S., Covalla, S. F., Woodard, T. L., and Lovley, D. R.: Biofilm and nanowire production leads to increased current in Geobacter sulfurreducens fuel cells, Appl. Environ. Microb., 72(11), 7345–7348, 2006.
Schink, B.: Energetics of syntrophic cooperation in methanotrophic degradation, Microbial Molecular Biology Review, 61, 262–280, 1997.
Schulz, H. D.: Quanitification of Early Diagenesis: Dissolved Constituents in Marine Pore Water, in: Marine Geochemistry, edited by: Schulz, H. D. and Zabel, M., 87–128, Springer, 2000.
Sørensen, K. B., Finster, K., and Ramsing, N. B.: Thermodynamic and kinetic requirements in anaerobic methane oxidizing consortia exclude hydrogen, actetate, and methanol as possible electron shuttles, Microb. Ecol., 42, 1–10, 2001.
Stewart, P. S.: Diffusion in biofilms, J. Bacteriol., 185(5), 1485–1491, 2003.
Strous, M. and Jetten, M. S. M.: Anaerobic oxidation of methane and ammonium, Annu. Rev. Microbiol., 58, 99–117, 2004.
Stumm, W. and Morgan, J. J.: Aquatic Chemistry: An Introduction Emphasizing Chemical Equilibria in Natural Waters, John Wiley and Sons, 1981.
Thauer, R. K., Jungermann, K., and Decker, K.: Energy conservation in chemotrophic anaerobic bacteria, Microbiol. Rev., 41, 100–180, 1977.
Treude, T., Orphan, V. J., Knittel, K., Gieseke, A., House, C. H., and Boetius, A.: Consumption of methane and CO2 by methanotrophic microbial mats from gas seeps of the anoxic Black Sea, Appl. Environ. Microb., 73, 2271–2283, 2007.
Valentine, D. L. and Reeburgh, W. S.: New perspectives on anaerobic methane oxidation, Environ. Microbiol., 2(5), 477–484, 2000.
Valentine, D. L.: Biogeochemistry and microbial ecology of methane oxidation in anoxic environments: a review, Anton. Leeuw. Int. J. G., 81, 271–281, 2002.
Wieland, A., de Beer, D., Damgaard, L. R., Kühl, M., and van Dusschoten, D.: Fine-scale measurement of diffusivity in a microbial mat with nuclear magnetic resonance imaging, Limnol. Oceanogr., 46(2), 248–259, 2001.

Table 1. Potential coupled reactions of AOM and SR discussed in Sørensen et al. (2001) and Valentine and Reeburgh (2000), and the corresponding standard free energy yield of the reactions, estimated using data from Stumm and Morgan (1981).

Reaction couples	ΔG^0 (kJ/mol)
Hydrogen transfer	
$CH_4 + 3H_2O \rightarrow HCO_3^- + H^+ + 4H_2$	229.1
$SO_4^{2-} + 4H_2 + H^+ \rightarrow HS^- + 4H_2O$	−262.0
Acetate transfer	
$CH_4 + HCO_3^- \rightarrow CH_3COO^- + H_2O$	14.8
$SO_4^{2-} + CH_3COO^- \rightarrow 2HCO_3^- + HS^-$	−47.7
Formate transfer	
$CH_4 + 3HCO_3^- \rightarrow 4HCOO^- + H^+ + H_2O$	154.0
$SO_4^{2-} + 4HCOO^- + H^+ \rightarrow 4HCO_3^- + HS^-$	−186.9

Table 2. Survey of available data on AOM/SR-mediating consortia sizes, cell sizes, and cell numbers.

consortia diameter[a] (µm)	inner core diameter[a] (µm)	layers of SRB in outer shell[b]	outer shell width[a] (µm)	ANME cell diameter[a] (µm)	SRB cell diameter[a] (µm)	# ANME cells in aggregate[c]	# SRB cells in aggregate[c]	SRB: ANME ratio	Ref.
3	2.2	1	0.4	0.5	0.4	63	189	3	A
6	4.4	2	0.8	0.5	0.4	504	1513	3	A
12	8.8	4	1.6	0.5	0.4	4034	12100	3	A
18	13.2	6	2.4	0.5	0.4	13616	40839	3	A
25	18.6	8	3.2	0.5	0.4	38094	106261	3	A
7.6	5.6	2.5	1	0.5	0.4	1040	3045	2.9	B
3.2	2.3	~1	0.45	0.5	0.4	72	238	3.3	C

A: Nauhaus et al. (2007); B: Knittel et al. (2005); C: Boetius et al. (2000)

[a] measured via microscopy

[b] derived by dividing the thickness of the SRB shell by the measured average diameter of a SRB cell

[c] derived by dividing the volume of an aggregate by the volume of a cell, assuming spherically shaped cells (r_{ANME}=0.5 µm, r_{SRB}=0.4 µm) and densest spherical packing.

Table 3. Properties of compounds considered in the model.

compound	D_{aq}^{a} $cm^2\ d^{-1}$	ΔG_f^{b} kJ/mol	activitiy coeff.[c]	boundary value[d], mM
H_2	2.272	17.55	1	10^{-7}–10^{-5}
HCO_3^-	0.593	−586.9	0.642	2
CH_4	0.860	−34.4	1	1–100
HS^-	1.026	12.1	0.604	1
$HCOO^-$	0.424	−351	0.604	10^{-7}–10^{-4}
CH_3COO^-	0.552	−369.4	0.642	10^{-7}–10^{-3}
SO_4^{2-}	0.550	−744.6	0.152	20

[a] diffusion coefficients from Schulz (2000)

[b] Free energy of formation values from Stumm and Morgan (1981). G_f^0 of H^+ and H_2O are 0 and −237.1 kJ/mol, respectively.

[c] estimated for an ionic strength of seawater.

[d] applicable in imposed concentration simulations; concentrations derived from growth experiments (Nauhaus et al., 2007).

Table 4. Model parameters.

Parameter	Description	Values/Units
$KmCH_4$	Half-saturation constant for methane in AOM	10% of [CH_4] at boundary, 0.1–10 mM
$KmEX$	Half-saturation constant for exchangeable species in SR	10^{-7} to 10^{2} mM
$KmSO_4$	Half-saturation constant for sulfate in SR	1 mM
R_{AOM}	Rate of AOM	Eq. (6), nmol cm^{-3} d^{-1}
R_{SR}	Rate of SR	Eq. (7), nmol cm^{-3} d^{-1}
k_{AOM}	Per cell turnover rate of methane by ANME	varied[a], fmol $cell^{-1}$ d^{-1}
k_{SR}	Per cell turnover rate of sulfate by SRB	varied[a], fmol $cell^{-1}$ d^{-1}
B_{ANME}	Cell density of ANME in inner core of consortia[b]	1.1×10^{16} cells l^{-1}
B_{SRB}	Cell density of SRB in outer shell of consortia[b]	2.2×10^{16} cells l^{-1}
F_{T-AOM}	Thermodynamic factor of AOM	0 to 1 [–]
F_{T-SR}	Thermodynamic factor of SR	0 to 1 [–]
$m\Delta G_{ATP}$	Minimum energy threshold	0–10 kJ/mol

[a] Estimates for rate constants are obtained from data in Nauhaus et al. (2007), assuming no substrate or thermodynamic limitations; cell specific rate in this experiment result in k_{AOM}~0.1–1 fmol $cell^{-1}$ d^{-1} are comparable to estimates from other data sets (10^{-4} to 10 fmol $cell^{-1}$ d^{-1}; Girguis et al., 2003, 2005; Knittel et al., 2005; Nauhaus et al., 2002; Orcutt et al., 2005).

[b] The number of cells within an aggregate was obtained by dividing the volume of the inner core and the outer shell by an estimate of the respective cell volumes and assuming densest even packing (Nauhaus et al., 2007), which resulted in 11.1 cells μm^{-3} in the inner core and 22.2 cells μm^{-3} in the outer shell, respectively (B_{ANME} and B_{SRB}).

BGD
5, 1933–1967, 2008

Table 5. Consortia size and abundance measured in ANME/SRB aggregates (agg.) enriched from Hydrate Ridge sediment at the beginning (Beg.) and end of the experiment (from Nauhaus et al., 2007). OD = outer diameter.

µm OD	# ANME agg.$^{-1}$	10^6agg. gws^{-1}		% aggregates		cells gws^{-1}		% cells	
		Beg.	End	Beg.	End	Beg.	End	Beg.	End
3	63	41	437	75	76	2.6×10^{9}	2.8×10^{10}	3	2
6	504	8	58	15	10	4.2×10^{9}	2.9×10^{10}	5	2
12	4034	3	33	5	6	1.2×10^{10}	1.3×10^{11}	13	9
18	13615	1.2	18	2	3	1.7×10^{10}	2.5×10^{11}	18	17
25	38094	1.5	26	3	5	5.6×10^{10}	9.9×10^{11}	61	69

Table 6. Maximum steady state concentrations of the intermediate compounds EX (nM) and the corresponding rate of AOM (R, expressed in units of 10^5 nmol gws^{-1} d^{-1}) calculated for various compounds in AOM/SR syntrophy mediated by a 3 µm diameter consortia. Values correspond to the experiments discussed in Figs. 3 and 4. Note that cell specific rates of AOM (k, in units of fmol cell^{-1} d^{-1}) are not constant but are those that lead to the highest R_{AOM} (see text).

ΔG_{ATP} (kJ/mol)	1			1			1			4			10		
CH_4 (mM)	100			19			1			19			19		
	k	EX	R	k	EX	R	k	EX	R	k	EX	R	k	EX	R
Acetate	1	200	6.6	0.1	40	0.85	0.01	2	0.07	0.01	11	0.1	0.001	1	0.01
Formate	0.01	35	0.13	0.01	20	0.12	0.001	11	0.013	0.01	13	0.11	0.001	9	0.013
Hydrogen	0.01	6	0.13	0.01	4	0.13	0.01	2	0.12	0.01	3	0.13	0.01	1	0.12

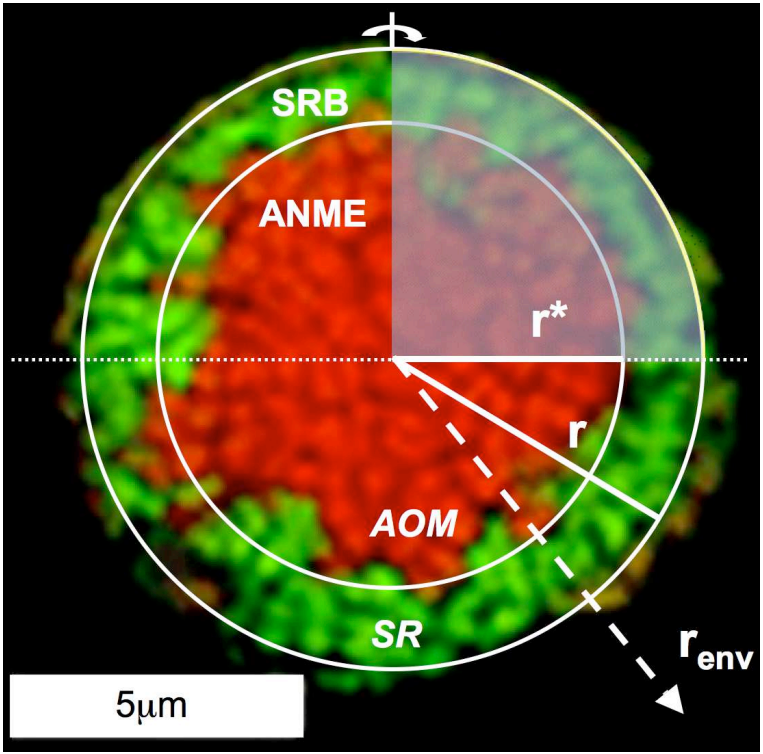

Fig. 1. AOM and SR mediating consortia, modified from Orphan et al. (2002). ANME (center, red) and SRB (shell, green) consortium from Eel River Basin methane-seep sediments surrounded by a layer of exopolymeric saccharide (yellow). The modeled geometrical arrangement is indicated by the white circles. The upper shaded quadrant denotes the model domain (with an inner aggregate radius r^*, an outer radius of the aggregate r and an environmental radius r_{env}), employing axial symmetry around the vertical axis, mirrored on the horizontal midsection plane denoted by the dotted horizontal line.

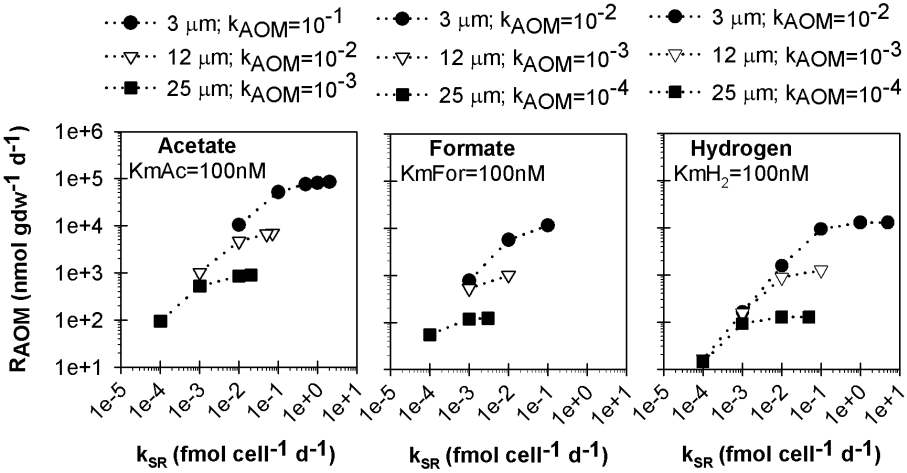

Fig. 2. Maximum rates of AOM calculated for variously sized aggregates (3, 12 or 25 μm OD) with each of the intermediate species acetate, formate, and hydrogen. For all simulations, methane was assumed to be 19 mM, the ΔG_{ATP} 1 kJ/mol, and K_mEX 100 nM. Note the different maximum cell specific AOM rates (k_{AOM}) for each size and intermediate species.

BGD
5, 1933–1967, 2008

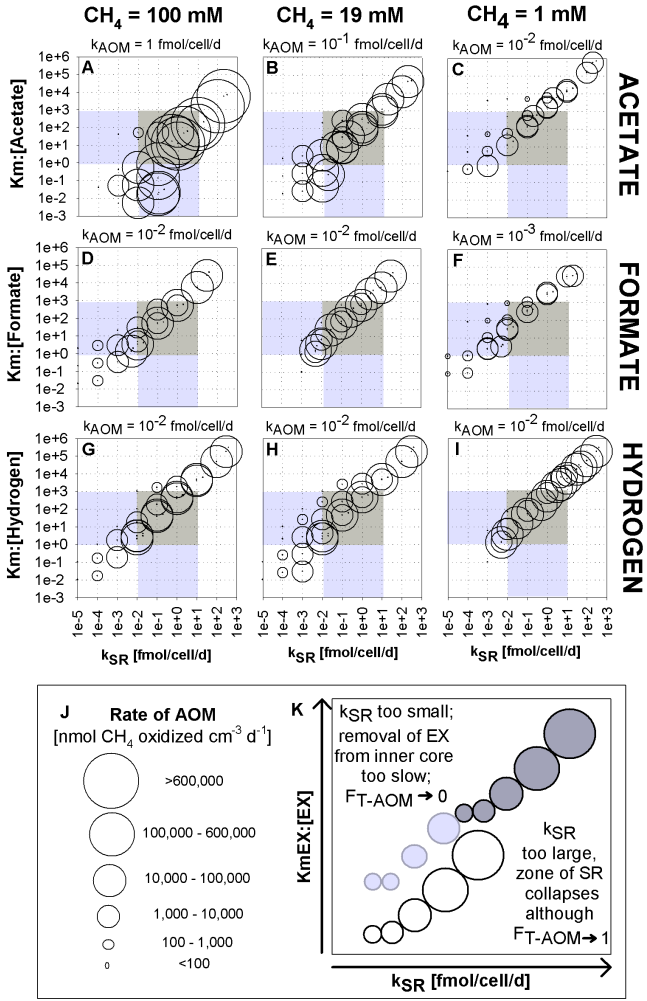

Fig. 3.

BGD
5, 1933–1967, 2008

Fig. 3. Rates of AOM averaged over the volume of the consortium for a 3 µm diameter aggregate under various concentrations of methane and assuming a minimum energy threshold of 1 kJ/mol (acetate, panels **A–C**; formate, panels **D–F**; and hydrogen, panels **G–I**) considered. Dots within symbols give the x-y coordinates, the size of the circle relates to magnitude of the rate; legend for symbols in panels (A)–(I) are given in panel **(J)**. Cell specific rates of SR (k_{SR}, in fmol cell^{-1} d^{-1}) are given on the x-axis; the scale is the same for panels (A)–(I) and is given in panels (G)–(I). The ratio of the half-saturation constant (Km) to the average steady state concentration of the intermediate species in the inner core (EX) is given on y-axis; scales are the same in all panels and are given in panels (A), (D) and (G). k_{AOM} values are given above each panel and represent those that lead to maximum AOM rates for each setting. Shaded regions in panels (A)–(I) indicated most realistic values as compared to experimental measurements. Panel **(K)** provides a diagram summary of how KmEX, k_{SR} and k_{AOM} affect the rate of AOM. At a fixed value of KmEX, an increase in k_{SR} leads to a larger rate of AOM and a lower average EX concentration, reflected in the sequences of open circles. A decrease in k_{AOM} results in a lower EX and lower rates of AOM for fixed values of KmEX and k_{SR}, as reflected in the transition from open to light grey filled circles. An increase in KmEX effectively reduces the rate of SR and increases EX concentration. When balanced by an increase in k_{SR}, this causes the transition from open to dark filled circles. Too high or too low values of k_{SR} lead to a shutdown of the aggregate either due to thermodynamic limiation of AOM or the collapse of the SR zone.

BGD

5, 1933–1967, 2008

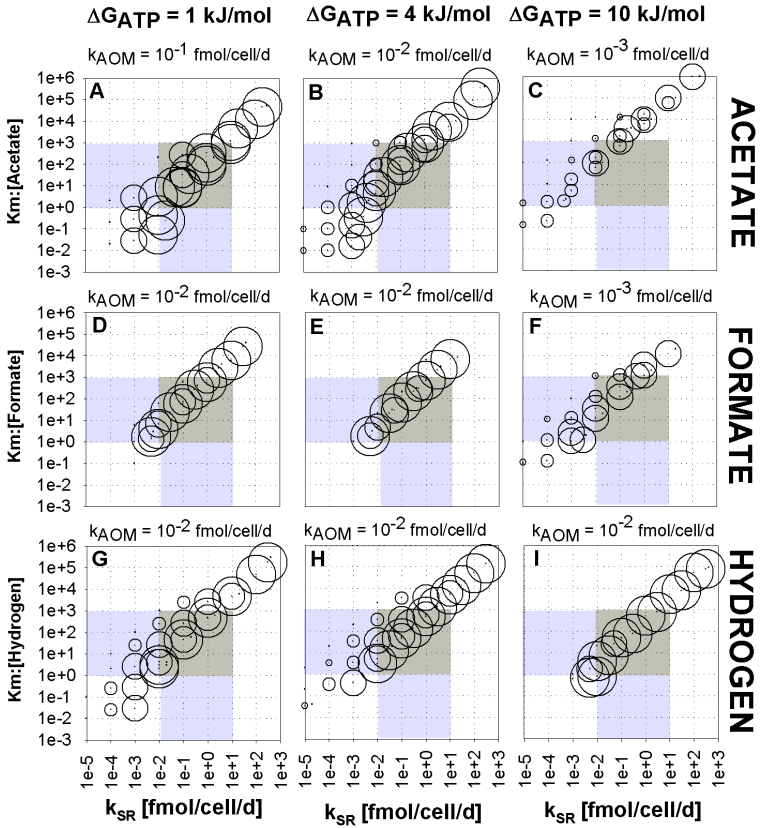

Fig. 4. Rates of AOM calculated using a 3 µm diameter aggregate under 19 mM methane concentration and various assumed minimum free energy thresholds (ΔG_{ATP} values) for each of the intermediate species (acetate, panels **A–C**; formate, panels **D–F**; and hydrogen, panels **G–I**) considered. Units and axes explained in Fig. 3 caption.

BGD
5, 1933–1967, 2008

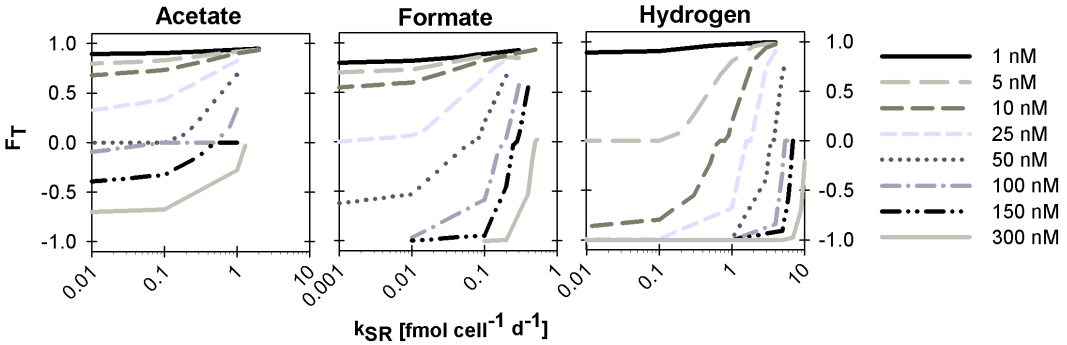

Fig. 5. Volume averaged values of F_T for a 3 µm OD consortia with fixed the environmental concentrations of the intermediate species (1–300 nM, as indicated in the legend). For all simulations, methane in the environment was assumed to be 19 mM, ΔG_{ATP}=1 kJ/mol, k_{AOM}=0.01 fmol cell^{-1} d^{-1}, and K_mEX=100 nM. Cell specific rates of SR (k_{SR}) are presented on x-axes (note scale differences between panels). F_T varies between −1 and 0 when $\Delta G_{methanogenesis}(=-\Delta G_{AOM})$ is more negative than the minimum energy quantum required for ATP production and methanogenesis becomes active. In an intermediate range, both forward and backward reaction are not feasible and the archaea are considered inactive ($F_{T-MG}=F_{T-AOM}=0$), while at more negative ΔG_{AOM}, methane gets oxidized, indicated by F_T ranging from 0 to 1 (Eq. 8). Right-hand end of lines indicate conditions where the zone of possible sulfate reduction collapses to zone smaller than a cell diameter.

BGD
5, 1933–1967, 2008